Liquid Crystals
Publication details, including instructions for authors and subscription information:
http://www.informaworld.com/smpp/title~content=t713926090

Light scattering from acrylate-based polymer dispersed liquid crystals: theoretical considerations and experimental examples

L. Leclercq

Online publication date: 06 August 2010

To cite this Article Leclercq, L.(1999) 'Light scattering from acrylate-based polymer dispersed liquid crystals: theoretical considerations and experimental examples', Liquid Crystals, 26: 3, 415 — 425
To link to this Article: DOI: 10.1080/026782999205191
URL: http://dx.doi.org/10.1080/026782999205191

LIQUID CRYSTALS, 1999, VOL. 26, NO. 3, 415–425

Light scattering from acrylate-based polymer dispersed liquid crystals: theoretical considerations and experimental examples

L. LECLERCQ†, U. MASCHKE‡*, B. EWEN†, X. COQUERET‡,
L. MECHERNENE§ and M. BENMOUNA§

†Max Planck Institut für Polymerforschung, Postfach 3148, D-55021 Mainz, Germany

‡Laboratoire de Chimie Macromoléculaire, UA CNRS N°351, Bâtiment C6, Université des Sciences et Technologies de Lille, F-59655 Villeneuve d'Ascq Cedex, France

§Université Aboubakr Belkaïd, Institut de Physique, Bel Horizon, BP 119, Tlemcen, Algeria

(*Received 14 July 1998; accepted 17 August 1998*)

A light scattering (LS) study made using acrylate-based polymer dispersed liquid crystals (PDLCs) is presented. The polarized component I_{VV} is measured for blends of a polyacrylate and the liquid crystal (LC) E7 at several compositions. Only the off-state configuration of the droplets with no external fields is considered here. These composites consist commonly of micron-sized nematic LC droplets dispersed in a solid polymer matrix. Theoretical expressions for the scattered intensities in the case of isotropic and anisotropic spherical droplets are given both in the Rayleigh–Gans approximation (RGA) and in the anomalous diffraction approximation (ADA). Series of VV and VH components of the scattering intensities are calculated using the models of Meeten, Stein and coworkers. The model calculations are compared with the light scattering data. This comparison enables us to extract information on the size and the shape of droplets assuming that the size distribution is uniform and that the scattering is due to single droplets, neglecting inter-particle correlation and multiple scattering effects. This paper demonstrates that the LS technique is a useful tool for studying the morphology of PDLC samples and estimating the average size of nematic droplets.

1. Introduction

Applications of polymer dispersed liquid crystals (PDLCs) are of particular interest in display systems [1–5]. These materials are made of nematic liquid crystal (LC) droplets dispersed in a polymer host and can scatter incident light with intensities that are controlled by applying an external electric field. The droplets are birefringent with an ordinary n_o and an extraordinary n_e refractive index, while the host polymer is generally chosen such that its refractive index n_m is approximately equal to n_o. In the absence of an external field, the droplet directors are randomly distributed giving rise to strong scattering of light to the extent that the PDLC film appears completely opaque. When an external electric field is applied, the directors are aligned and the incident light at right angles is basically sensitive to the refractive index n_o only. In these conditions, the droplets scatter light very weakly and the system becomes transparent. This behaviour is extremely useful in the design of switchable windows and display systems.

PDLCs are prepared in our laboratory by the method of polymerization-induced phase separation (PIPS) [6–9]. Reactive solutions made of mixtures of monomers, oligomers and nematic LCs are exposed to electron beam radiation. Crosslinking-polymerization takes place simultaneously and leads to phase separation of the polymer and the LC.

Light scattering from mixtures of nematic droplets and polymers is a relatively new topic and the theories associated with this problem use in general the Rayleigh–Gans [10, 11] or the anomalous diffraction [12] approximations. The basic theories for anisotropic droplets were developed by Stein and Rhodes [13] and Meeten and Navard [14–17] and later applied to PDLC systems by Zumer [18–20], Whitehead [21, 22], Yang [23, 24], Montgomery [25, 26] and others [27–29]. For

*Author for correspondence.

example, Whitehead and Meeten calculated the total cross section for nematic droplets with and without an electric field, while Stein and Meeten derived the polarized and depolarized intensities I_{VV} and I_{VH} and their corresponding angular gains $(4\pi r^2/AI_0)I_{VV}$ and $(4\pi r^2/AI_0)I_{VH}$ where A is the cross sectional area of the scattering object projected onto the incident beam whose intensity is I_0, and r is the distance between the sample and the detector. Meeten *et al.* considered the results for isotropic and anisotropic spherical droplets and observed that the Rayleigh–Gans and anomalous diffraction approximations agree quite well for anisotropic spheres with a mean refractive index close to that of the host polymer.

The LS technique consists of illuminating the sample with linearly polarized light, and examining the scattered intensity after the light has passed through an analyser placed with its plane normal to the incident beam (see figure 1) [30, 31]. Two main arrangements were considered: the VV mode where the analyser axis is parallel to the polarization direction of the incident beam and the VH mode for which the analyser axis is at right angles with the polarization direction.

In this paper, we briefly recall the formulae for the scattering intensities commonly used in the case of isotropic and anisotropic spheres. We perform a comparative study between the scattering curves in various conditions as functions of the amplitude of the wave vector **q**, using refractive indices characterizing the PDLC system under consideration. The ratio $I_{VV}(\mathbf{q})/I_{VV}(\mathbf{q}=0)$ has been calculated in both the RGA and the ADA and the results have been compared with the experimental data. This enables us to study the sample morphology and extract information on the size and the shape of the droplets. The theoretical variation of the depolarized intensity as a function of **q** is briefly discussed for isotropic spheres just for a comparison with the curve of I_{VV}. Since our LS measurements are performed in the absence of external fields, the signal for I_{VH} is extremely weak and therefore we did not consider its detailed investigation here. We limit ourselves to the comparison of LS data and theoretical results in different models and approximations.

2. Experimental

2.1. *Materials*

The LC mixture E7 (Merck Ltd, UK) was used during this work. The indices of refraction of this mixture are given in equation (6) and related by $n_t = n_0$ and $n_r = n_e$. The prepolymer chosen consists of an aromatic polyester acrylate (Rahn AG, Switzerland) diluted with additional monomers including tripropyleneglycol diacrylate (UCB, Belgium). The refractive indices of the cured prepolymer/LC blends in the LC concentration range below the limit of phase separation have been previously determined [32]. Under the curing conditions chosen in our case, roughly 20 wt % of LC remains dissolved in the polymer matrix [8]. As a consequence, the effective refractive index of the polymer matrix increases compared with that of the prepolymer cured in the absence of LC. The refractive index of the transparent cured film based on 80 wt % prepolymer/20 wt % LC is $n_p = 1.5269$ ($\lambda = 632.8$ nm) [32].

2.2. *Preparation of PDLC films*

(100-x) wt % of the prepolymer ($x = 30, 40, 50$) and x wt % of the LC were mixed together at room temperature until the mixtures became homogeneous. Several samples were prepared for each composition by sandwiching the initial reactive mixture between a glass plate (Balzers, Liechtenstein) and a 100 μm thick poly(ethyleneterephthalate) sheet (Renker, Germany), both coated with a thin layer of conducting indium/tin oxide. The thickness of the composite films was controlled by using 25 μm thick spacers (double sided adhesive strips, 3M, France).

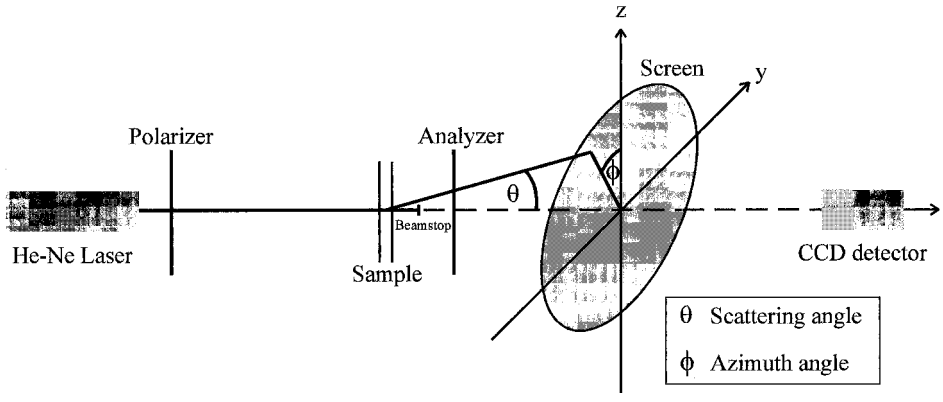

Figure 1. Experimental set-up of the light scattering apparatus showing the scattering and azimuthal angles.

2.3. *Electron beam curing*

The electron beam generator used to prepare the PDLC samples by a PIPS process was an Electrocurtain Model CB 150 (Energy Sciences Inc., USA) with an operating high voltage of 175 kV. This value was increased to 190 kV to allow a uniform penetration of the applied dose into the depth of the samples. The sandwiched composite materials were placed in a sample tray, which was passed beneath an inert atmosphere under the accelerated electron curtain on a conveyor belt. The applied dose of 60 kGy was achieved by using a beam current of 4 mA and a conveyor speed of $0.22\ \mathrm{m\ s^{-1}}$. These values have not been changed during the experiments in order to apply the same curing conditions each time. No temperature control during the irradiation process was applied.

2.4. *Light scattering*

Light scattering measurements were performed at room temperature using the set-up illustrated in figure 1. The He-Ne Laser ($\lambda = 632.8$ nm) was polarized perpendicular to the scattering plane. In order to measure the I_{VV} component the analyser was kept parallel to the polarizer and a beam stop prevented the transmitted beam from reaching the screen. The scattering pattern was recorded by a CCD camera. For I_{VV} a ϕ-independent circular intensity pattern was found allowing performance of radial averages of the scattered intensity.

3. Theoretical expressions for the scattering intensities

Following the scattering formalism developed by van de Hulst [12], the components of the scattered intensity can be derived in general from the scattering matrix $\boldsymbol{S}$

$$\boldsymbol{S} = \begin{pmatrix} S_2 & S_3 \\ S_4 & S_1 \end{pmatrix}. \tag{1}$$

The expressions for the scattering intensities are greatly simplified by considering spherical particles. In this case, the off-diagonal elements of the matrix $\boldsymbol{S}$ are zero and the intensities are uniquely expressed in terms of S_1 and S_2 [12, 14]

$$I_{VV} = \frac{I_0}{k^2 r^2} |S_1 \sin^2 \phi + S_2 \cos^2 \phi|^2 \tag{2}$$

$$I_{VH} = \frac{I_0}{k^2 r^2} |(S_2 - S_1) \sin \phi \cos \phi|^2 \tag{3}$$

The experimental set-up of figure 1 shows the position of the azimuthal angle ϕ and the scattering angle θ. In equations (2) and (3), $k = 2\pi/\lambda$ and λ is the optical wavelength of the incident beam. The matrix elements S_1 and S_2 depend upon the optical geometry and the approximation appropriate for the system under consideration.

3.1. *The Rayleigh–Gans approximation (RGA)*

The RGA provides a model of light scattering appropriate to systems where the induced maximum phase shift remains weak [10, 11]. Each volume element of the scattering object acts as a dipole which scatters light according to the theory of Rayleigh. All elements of the scattering volume behave as independent dipoles. This gives rise to the RGA model which is valid under the following conditions only

$$\left| \frac{n_{LC}}{n_m} - 1 \right| \ll 1 \qquad 2kR \left| \frac{n_{LC}}{n_m} - 1 \right| \ll 1 \tag{4}$$

where R is the radius of the scattering object or droplet, n_m is the refractive index of the matrix polymer and n_{LC} is the mean effective refractive index of the liquid crystal. The latter quantity is defined in terms of the indices of refraction n_0 and n_e following

$$n_{LC} = \left(\frac{n_e^2 + 2n_0^2}{3} \right)^{1/2}. \tag{5}$$

The first condition in the inequalities (4) means that the average refractive indices n_m and n_{LC} should remain close to each other. This means that the incident wave does not undergo large changes of phase and amplitude inside the particle and the electric field can be correctly approximated with the field of the incident beam. The second condition means that the size of the droplet must be much smaller than the wavelength of the incident beam implying that the Rayleigh–Gans theory is suitable for relatively small particles.

The polyacrylate/E7 system under investigation has the following indices of refraction

$$n_m = 1.5269 \quad n_0 = 1.5183 \quad n_e = 1.7378 \quad n_{LC} = 1.5948. \tag{6}$$

This value of n_m was measured in our laboratory at $T = 20°C$ and wavelength $\lambda = 632.8$ nm [32], while the indices of refraction of E7 were provided by the manufacturer (Merck) [33]. Although these indices of refraction characterize E7 in the pure state, they will be adopted assuming that they remain unchanged for the polyacrylate/E7 system. According to equations (4–6), the droplet diameter $D = 2R$ should not exceed 0.2 μm for the corresponding optical softness of the object. In particular, if the difference between n_{LC} and n_m is smaller than 0.2, the droplet diameter may be larger than 0.2 μm. But in this case, the scattering signal should be limited to the range of angles using the LS techniques.

The investigation of LS by small, anisotropic objects dispersed in a polymer matrix was first reported by Stein and Rhodes [13] using the RGA. These authors applied the model to crystalline spherulites built within an amorphous bulk polymer. Their model predicts that

$I_{VH} = 0$ for isotropic spherulites, somewhat in contrast with experimental findings [15] for polymer latex particles. These isotropic spheres show a four-leaf-clover LS VH pattern and resemble those of crystalline polymers observed in polyethylene. In view of the fact that the LS technique is a powerful tool for studying morphology and considering that its application to PDLC systems is relatively new, we think that it is worthwhile examining the problem here, looking at the predictions of different LS theories for spherulites and comparing the results with experimental data for the polyacrylate/E7 systems.

Theoretically, Meeten *et al.* [14, 16] obtained the elements of the matrix $\boldsymbol{S}$ for three dimensional spherulites from the method of Stein and Rhodes [13]. They represented these objects by homogeneous spheres with radial and tangential refractive indices. In the case of anisotropic spheres, this model gives

$$S_1 = \frac{2ik^3R^3}{3}[3(\mu-1)f_1 + \Delta\mu f_2] \tag{7}$$

$$S_2 = \frac{2ik^3R^3}{3}\left[3(\mu-1)f_1\cos\theta - \Delta\mu f_2\left(1+\cos^2\frac{\theta}{2}\right)\right] \tag{8}$$

where $\mu = (n_r + 2n_t)/3n_m = \langle n\rangle/n_m$ and the mean refractive index of the LC $\langle n\rangle$ should not be confused with n_{CL} defined in equation 5; $\Delta\mu = (n_r - n_t)/n_m$ is the optical anisotropy relative to n_m, and n_r and n_t are the radial and tangential refractive indexes of the sphere, respectively. The quantities u, f_1, and f_2 introduced here are

$$u = 2kR\sin(\theta/2) \qquad f_1 = \frac{\sin u - u\cos u}{u^3}$$

$$f_2 = \frac{u\cos u - 4\sin u + 3\int_0^u \frac{\sin t}{t}\mathrm{d}t}{u^3}. \tag{9}$$

Combining these results, one obtains the following scattering intensities

$$I_{VV} = C\left((\mu-1)f_1 + \frac{\Delta\mu}{3}f_2 - \left[2(\mu-1)f_1\sin^2\frac{\theta}{2} + \frac{\Delta\mu}{3}f_2\left(2+\cos^2\frac{\theta}{2}\right)\right]\cos^2\phi\right)^2 \quad \text{(Meeten } et\ al.\text{)} \tag{10}$$

$$I_{VH} = C\left[2(\mu-1)f_1\sin^2\frac{\theta}{2} + \frac{\Delta\mu}{3}f_2\left(2+\cos^2\frac{\theta}{2}\right)\right]^2 \times \sin^2\phi\cos^2\phi \quad \text{(Meeten } et\ al.\text{)} \tag{11}$$

where the constant factor C is given by

$$C = I_0\left(\frac{2k^2R^3}{r}\right)^2. \tag{12}$$

Stein *et al.* [13] obtained quite different results for spherulites of crystalline polymers within the same approximation. These results are recalled for the sake of comparison

$$I_{VV} = C\left[(\mu-1)f_1 + \frac{\Delta\mu}{3}f_2 - \Delta\mu f_2\cos^2\left(\frac{\theta}{2}\right)\cos^2\phi\right]^2 \quad \text{(Stein } et\ al.\text{)} \tag{13}$$

$$I_{VH} = C\left[\Delta\mu f_2\cos^2\frac{\theta}{2}\right]^2\sin^2\phi\cos^2\phi \quad \text{(Stein } et\ al.\text{)}. \tag{14}$$

As pointed out earlier, the theory of Stein *et al.* has a historical importance with regard to the models developed for the study of scattering by PDLC systems. The two sets of equations (10, 11) and (13, 14) are quite different. In particular, for isotropic spheres $\Delta\mu = 0$ and these equations become

$$I_{VV} = C\left[(\mu-1)f_1 - 2(\mu-1)f_1\sin^2\frac{\theta}{2}\cos^2\phi\right]^2 \quad \text{(Meeten } et\ al.\text{, isotropic)} \tag{15}$$

$$I_{VH} = C\left[2(\mu-1)f_1\sin^2\frac{\theta}{2}\right]^2\sin^2\phi\cos^2\phi \quad \text{(Meeten } et\ al.\text{, isotropic)} \tag{16}$$

and

$$I_{VV} = C[(\mu-1)f_1]^2 \quad \text{(Stein } et\ al.\text{, isotropic)} \tag{17}$$

$$I_{VH} = 0 \quad \text{(Stein } et\ al.\text{, isotropic)}. \tag{18}$$

For a weakly anisotropic spherulite having a small refractive index mismatch with its surrounding, the two models of Stein *et al.* and Meeten *et al.* predict different I_{VV} and I_{VH} curves. Unlike Stein *et al.*, Meeten *et al.* predict that the depolarized component I_{VH} is zero for isotropic spheres. Note that the I_{VV} and I_{VH} patterns are usually attributed to the spherulite anisotropy and crystallinity. The fact that these quantities are non-zero for isotropic spheres is consistent with the experimental observations.

It would be interesting to perform a more systematic analysis of the scattering signal under various conditions and compare the predictions with the scattering data. We choose to normalize the intensity with respect to the value at zero scattering angle and consider the variation of the intensity with the amplitude of the scattering vector $\mathbf{q}$. In the theoretical formulae, the absolute intensity

involves the constant C which depends on the droplet radius. This quantity is obtained from the full scattering curve showing the variation of the intensity with the wave-vector $\mathbf{q}$, and therefore, it is not *a priori* known. Moreover, the scattering intensity at small angles encounters the problem of the incident beam and requires a beam-stop. The same normalization is used for all figures portraying LS data where the forward scattering intensity was determined by extrapolation of the data to $\mathbf{q} = 0$ limit, using a least square fit. Figure 2 represents the variation of the polarized component $I_{VV}(\mathbf{q})/I_{VV}(\mathbf{q} = 0)$ with the amplitude of the wave vector $\mathbf{q}$ for isotropic spheres of three radii 0.5, 1 and 2 μm. The predictions of the models of Meeten *et al.* and Stein *et al.* are represented on this figure for the sake of comparison. The scattering signal is quite sensitive to the droplet size in both models. As the radius increases, interference between scattered waves get stronger and leads to a large decrease of the signal. If the sphere radius is equal to or less than 1 μm, the two models predict slightly different results. The model of Stein *et al.* gives a slightly higher signal. For a sphere of 2 μm radius, the scattering curves are superimposed. Furthermore, a change of the azimuthal angle ϕ from 45° to 0° leads to a small shift in the curve downward in the case of a sphere of 0.5 μm radius and likewise in the Meeten model. All the other systems considered here show no sensitivity to the azimuthal angle ϕ.

One of the main goals of the present investigation is to understand the effects of anisotropy on the scattering signal. For this reason, we represent in figure 3 the variation of $I_{VV}(\mathbf{q})/I_{VV}(\mathbf{q} = 0)$ as a function of $\mathbf{q}$ for anisotropic spheres including the anisotropic contributions shown in equations (10–13). One immediately observes oscillations for the anisotropic sphere of highest radius. These oscillations are highly damped when the sphere radius decreases. Quantitatively, the signals for isotropic and anisotropic spheres are quite different as we can see by superimposition of figures 2 and 3. Curves shift to the left when the radius increases indicating that the signal is depressed.

Besides the oscillations, the scattering signal does not undergo substantial changes upon introduction of anisotropic effects. This is somewhat overestimated in the

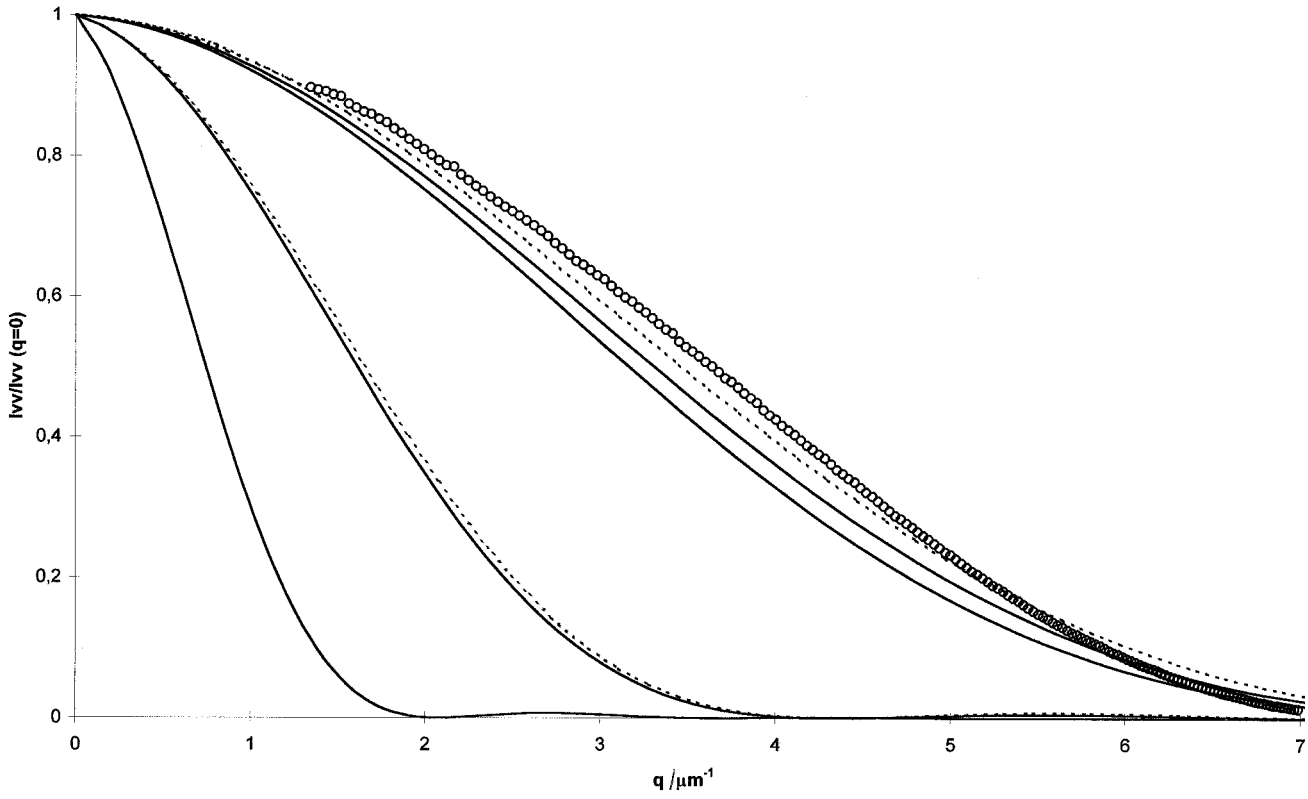

Figure 2. Variation of the scattering intensity $I_{VV}(\mathbf{q})/I_{VV}(\mathbf{q} = 0)$ as a function of $\mathbf{q}$ for isotropic spheres with different radii in the RGA. The continuous curves represent the Meeten *et al.* model, while the dashed curves represent the Stein *et al.* model for spheres of different radii. The curves are plotted for the following conditions from left to right, respectively: (R = sphere radius, ϕ = azimuthal angle) $R = 2\,\mu m$, $\phi = 0$ and 45° (Meeten and Stein); $R = 1\,\mu m$, $\phi = 0$ and 45° (Meeten); $R = 1\,\mu m$, $\phi = 0$ and 45° (Stein); $R = 0.5\,\mu m$, $\phi = 0$ (Meeten); $R = 0.5\,\mu m$, $\phi = 45°$ (Meeten); $R = 0.5\,\mu m$, $\phi = 0$ and 45° (Stein). The symbol ○ represents the light scattering data for the polyacrylate/E7 system at 70 wt % of LC.

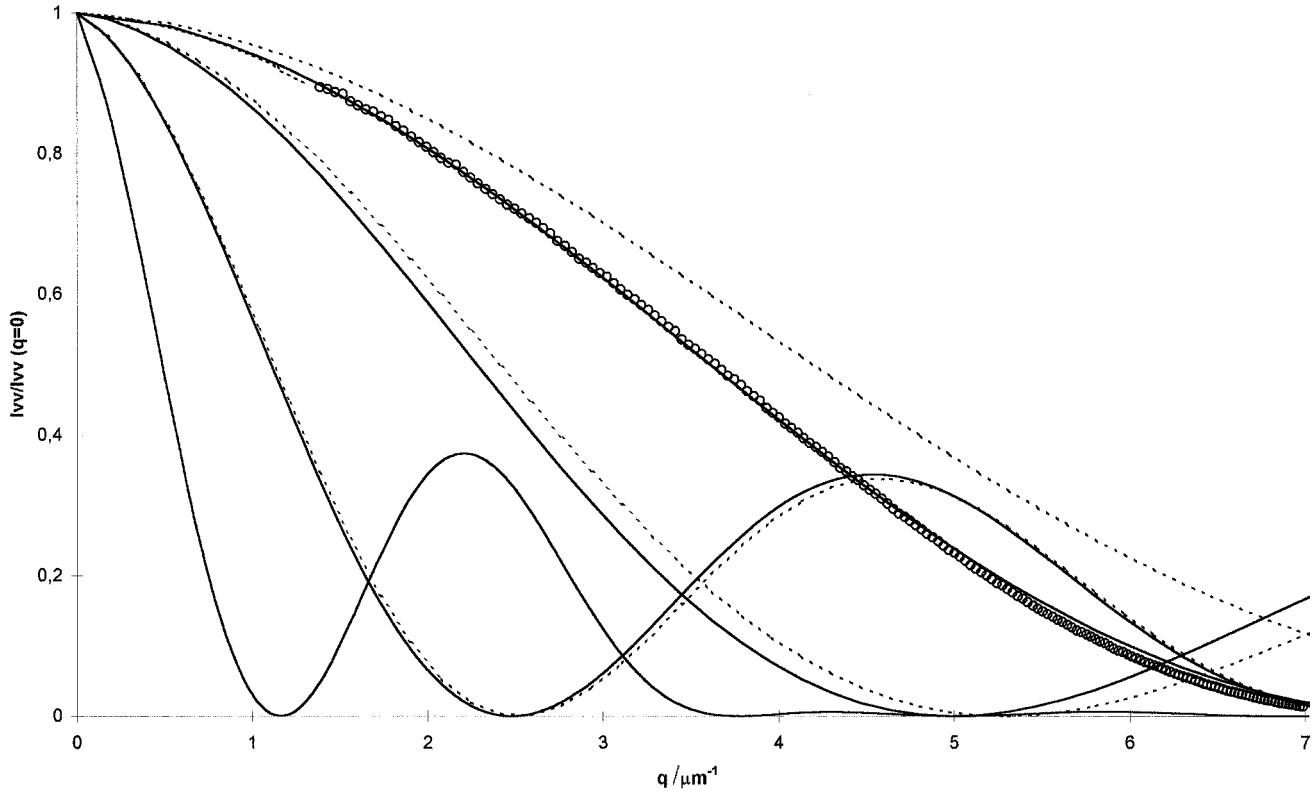

Figure 3. Variation of the scattering intensity $I_{VV}(\mathbf{q})/I_{VV}(\mathbf{q}=0)$ as a function of $\mathbf{q}$ for anisotropic spheres with different radii in the RGA, at an azimuthal angle $\phi = 0$. The continuous curves represent the Meeten *et al.* model, while the dashed curves represent the Stein *et al.* model for spheres of different radii. The curves are plotted for the following conditions from left to right, respectively: (R = sphere radius) $R = 2\,\mu$m, (Meeten and Stein); $R = 1\,\mu$m, (Meeten); $R = 1\,\mu$m, (Stein); $R = 0.5\,\mu$m, (Meeten); $R = 0.5\,\mu$m, (Stein); $R = 0.3\,\mu$m, (Meeten); $R = 0.3\,\mu$m, (Stein). The symbol ○ represents the light scattering data for the polyacrylate/E7 system at 70 wt % of LC.

Stein *et al.* model for radius 0.5 µm, while for larger spheres, the signal is practically the same compared to the results of Meeten *et al.* The influence of the azimuthal angle ϕ is the same as in the case of isotropic spheres. The curve shifts slightly upward in the Meeten *et al.* model for the smallest sphere when ϕ is increased from 0° to 45°. Since this is exactly the behaviour observed in figure 2, we do not show a curve for the effect of azimuthal angle for anisotropic spheres.

Another interesting quantity useful for the analysis of the morphology of nematic droplets is the depolarized component of the scattering signal denoted $I_{VH}(\mathbf{q})$. Figure 4 represents the variations of the normalized intensity $I_{VH}(\mathbf{q})/I_{VHmax}$ versus $\mathbf{q}$ for isotropic spheres having the same size as in the previous figures in model of Meeten *et al.* at $\phi = 45°$, normalized with respect to the maximum value. The maximum intensity does not take place at the same $\mathbf{q}$ value for different sizes. The normalization used previously is not applicable here since the depolarized signal vanishes at $\mathbf{q} = 0$. This normalization is convenient, but has the drawback of making comparison of scattering intensities for different spheres more difficult. The oscillations shown in this figure are much more significant than those due to anisotropy in the polarized component $I_{VV}(\mathbf{q})$ (figure 3). The number of oscillations increases with the droplet size, suggesting that one could relate the period of oscillations $\mathbf{q}_0^{-1}$ to the droplet diameter $D \equiv 2R$ by the relationship $D = 2\pi/\mathbf{q}_0$. Within a reasonable accuracy, this is indeed the case. Moreover, when the radius increases, the signal shifts to lower $\mathbf{q}$ values in a similar way to the polarized component for both isotropic and anisotropic spheres.

3.2. *The anomalous diffraction approximation (ADA)*

The anomalous diffraction approximation replaces the three dimensional object by a two dimensional plate-like object which collects information about the phase of the incident light [12]. Two conditions must be satisfied in the ADA:

$$kR \gg 1 \qquad \left|\frac{n_{LC}}{n_m} - 1\right| \ll 1. \tag{19}$$

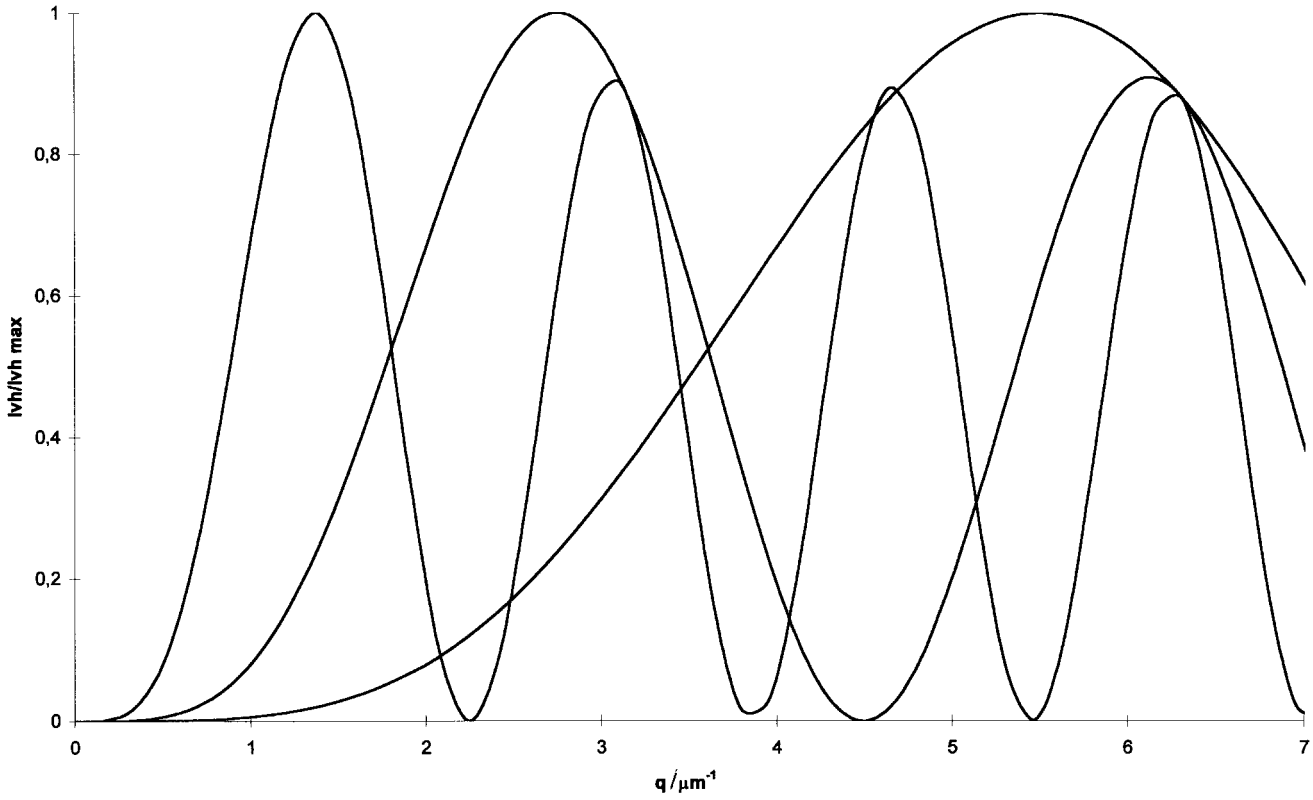

Figure 4. Variation of the scattering intensity $I_{VH}(\mathbf{q})/I_{VHmax}$ as a function of $\mathbf{q}$ for isotropic spheres in the model of Meeten *et al.* with the RGA at $\phi = 45°$. The curves are plotted for the following conditions from left to right, respectively: (R = sphere radius) $R = 2, 1, 0.5\,\mu m$.

The first condition tells us that the droplet radius is much larger than the wavelength of the incident beam. The second conditions insures that the refraction and reflection at the nematic/polymer interface can be neglected. The nematic droplet produces a phase shift in the incident light changing neither its intensity nor its direction. In the far-field limit, the light scattering distribution is similar to a Fraunhofer diffraction pattern. There are two contributions: the first contribution uses the Babinet principle and is deduced from the light scattered by an opaque object; the second contribution arises from the light undergoing a phase shift Δ and depends on the size and orientation of the nematic droplets.

The ADA is appropriate for large particles, with a size larger than the wavelength of the incident beam, and for the systems under consideration here according to the refractive indices given in equation (6). Typically, the droplet radius should be larger than $0.2\,\mu m$.

In the case of isotropic spheres, the ADA has been worked out by various authors, and in particular by Meeten *et al.* [14, 17] who reported the following results for the van de Hulst matrix elements

$$S_1 = k^2 R^2 \int_0^1 [1 - \exp(-2i\Delta)] J_0(ux)x\,dx \qquad (20)$$

$$S_2 = S_1 \cos\theta. \qquad (21)$$

The phase shift is given by

$$\Delta = kR(\mu - 1)(1 - x^2)^{1/2} \qquad (22)$$

where $J_0(x)$ is the zero order Bessel function [34]. For anisotropic spheres, it is convenient to split S_1 and S_2 in order to distinguish explicitly the terms expressing isotropic and anisotropic effects. Meeten *et al.* suggest [14]:

$$S_1 = S_{isotrop} + S_{anisotrop} \qquad (23)$$

$$S_2 = (S_{isotrop} - S_{anisotrop}) \cos\theta \qquad (24)$$

where the isotropic term is

$$S_{isotrop} = k^2 R^2 \int_0^1 i(x)\,dx \qquad (25)$$

with

$$i(x) \approx \left\{1 - \frac{1}{2}\left[\exp\left(-2ikR\frac{n_t}{n_m}(1-x^2)^{1/2}\right) + \exp\left(-2ikR\left(\left(\frac{n_t}{n_m}-1\right)(1-x^2)^{1/2} - \Delta\mu x \arctan\left(\frac{1}{x^2}-1\right)^{1/2}\right)\right)\right]\right\} J_0(ux)x \tag{26}$$

while the anisotropic term has the form

$$S_{\text{anisotrop}} = \frac{k^2R^2}{2}\int_0^1 a(x)\,dx \tag{27}$$

with the function $a(x)$ given by

$$a(x) \approx \left\{\exp\left[-2ikR\frac{n_t}{n_m}(1-x^2)^{1/2}\right] - \exp\left[-2ikR\left(\left(\frac{n_t}{n_m}-1\right)(1-x^2)^{1/2} - \Delta\mu x \arctan\left(\frac{1}{x^2}-1\right)^{1/2}\right)\right]\right\} J_2(ux)x \tag{28}$$

where $J_2(x)$ represents the second order Bessel function [34]. The expressions of $i(x)$ and $a(x)$ are obtained from the extension of the phase lag functions in powers of the anisotropy $\Delta\mu$, keeping linear terms only. Figure 5 represents the variation of $I_{VV}(\mathbf{q})/I_{VV}(\mathbf{q}=0)$ as a function of $\mathbf{q}$ for the same isotropic spheres as those in figure 2. We have chosen a similar representation to make comparison with the RGA results possible. These results clearly show that the polarized signal is qualitatively the same regardless of the approximation used. Essentially all the remarks made in figure 2 remain valid in the present case with the observation that the ADA systematically predicts slightly higher values with a decreasing discrepancy when $\mathbf{q}$ increases.

4. Results and discussions

As explained earlier, figures 2–5 show the theoretical results for the scattering intensity as a function of $\mathbf{q} = 4\pi/\lambda \sin\theta/2$ for several sphere radii. To plot the theoretical curves, one needs to characterize the mean refractive index and the optical anisotropy of the LC droplet relative to the polymer, denoted μ and $\Delta\mu$, respectively, but these quantities are defined in terms of

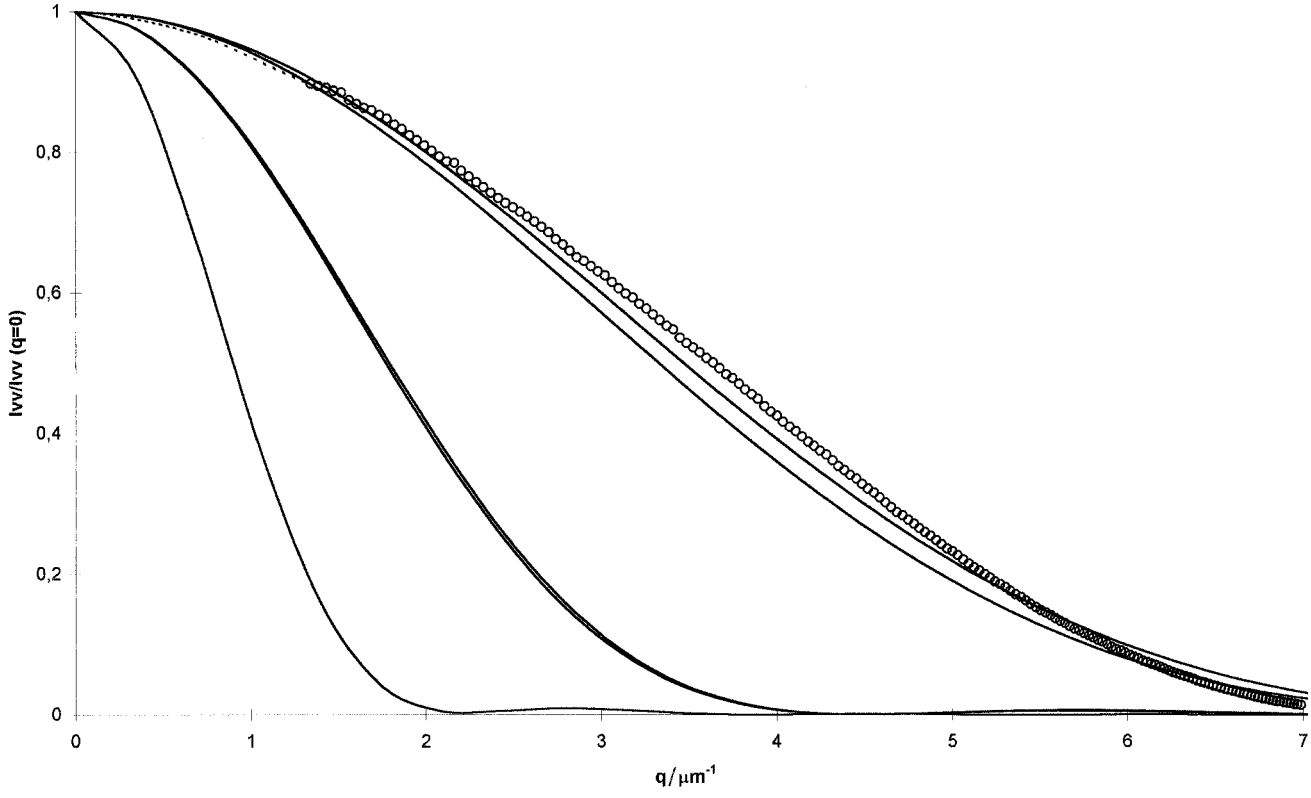

Figure 5. Variation of the scattering intensity $I_{VV}(\mathbf{q})/I_{VV}(\mathbf{q}=0)$ as a function of $\mathbf{q}$ for isotropic spheres with different radii in the Meeten model with the ADA. The curves are plotted for the following conditions from left to right, respectively: (R = sphere radius, ϕ = azimuthal angle) $R = 2\,\mu m$, $\phi = 0$ and 45°; $R = 1\,\mu m$, $\phi = 0$ and 45°; $R = 0.5\,\mu m$, $\phi = 0°$; $R = 0.5\,\mu m$, $\phi = 45°$. The symbol ○ represents the light scattering data for the polyacrylate/E7 system at 70 wt % of LC.

tangential and radial refractive indices. Since the only indices of refraction available for E7 are n_0 and n_e, we make the following identification $n_t = n_0$ and $n_r = n_e$ which is also used by others [28]. This identification is not rigorously true in general and can be applied only in certain cases of droplet geometry and optical symmetry. In figures 2, 3 and 5, we included the scattering data for the highest composition of 70 wt % of LC by the symbol ○ . The polarized component of the scattering intensity I_{VV} has been measured for a wide range of angles from 6° to 30°. According to the expression for $\mathbf{q}$ and the wavelength used, this corresponds to $\mathbf{q}$-values spanning the range from 1 to 7 μm^{-1}. Below 6°, no measurements were made and the results were extrapolated by a least square fit to obtain the value at zero angle; this is needed for the normalization procedure and comparison with the theoretical predictions. The region between 0 and 1 μm^{-1} is not covered by the experiments and is represented by dotted lines. By putting experimental data together with theoretical results, one wishes to see which approximation is more appropriate for the system and obtain valuable information on the geometry, the anisotropy and the size of the droplets. Figures 2 and 5 show that the data are well represented within either the RGA or the ADA for isotropic spheres of radius 0.5 μm, although the fit with the ADA seems better. It is worthwhile recalling that one of the conditions for the validity of the ADA is that the sphere radius should be larger than 0.2 μm, which is consistent with the observed size. However, the size of the droplets found under the present conditions is in the range where the two approximations give comparable results and it is quite difficult to make a clear distinction between them to judge which one is more suitable.

The fact that the theoretical curves predict slightly lower values indicates that the droplet mean radius is probably a little lower than 0.5 μm. From such observations, one is tempted to conclude that the droplets are indeed isotropic spheres. Figure 4 shows the same data for the PDLC system with the LC composition at 70 wt %. Here, we added the theoretical curves for isotropic spheres of radius 0.3 μm in the Meeten *et al.* and Stein *et al.* models. The reason is clear since one observes that the data are well represented by the model of Meeten *et al.*, while the model of Stein *et al.* predicts slightly higher values over the whole range of $\mathbf{q}$ covered by the experiments. This means that the droplets at this composition can also be represented by anisotropic spheres of radius 0.3 μm and that the model of Meeten *et al.* with the RGA is also a good candidate for the characterization of the droplet configuration.

In order to see whether the normalized scattering intensity changes with the LC composition, we represent in figure 6 the data obtained by the same experimental procedure for three PDLC films with different LC compositions of 70, 60 and 50 wt %. One observes that the normalized intensity is practically the same for 70 and 60 wt %, but the intensity for the lowest composition is much more depressed. It is interesting to correlate this observation with the results of the transmitted light for the same samples shown in the inset of this figure [8]. The intensity of transmitted light is practically zero for the PDLC films containing 70 and 60 wt % LC, while that for the 50 wt % sample is much more important. This observation is consistent with the fact that the relative scattering is the same for the former two samples, while for the latter sample the scattering is quite low. The fact that the scattering intensity signal changes with the composition may be an indication that inter-droplet correlation is not negligible in this range of composition. In [8], it was suggested that this correlation is so strong that large aggregates of droplets may be formed. Such correlations are completely neglected in all the theoretical models used here. It is worth mentioning that scanning electron microscopy measurements were performed on films corresponding to 50 wt % LC. These measurements showed that the droplets present an ellipsoidal form with an axial ratio of 0.6 and a major axis of 0.5 μm, which is consistent with the sphere radius obtained from the light scattering data. The textures observed microscopically indicated that the droplet shape and size do not change with composition and only their number density increases.

5. Conclusion

This paper reviews briefly some theoretical results describing the scattering properties of PDLC systems in various models and approximations. In particular, the models of Stein *et al.* and Meeten *et al.* are discussed within the RGA and ADA. The variations of the scattering intensities with the wave vector $\mathbf{q}$ are calculated for various conditions and their changes with the sizes of the scattering object are characterized. To check the validity of these models, LS measurements were performed using PDLC systems made of polyacrylate/E7 mixtures prepared in our laboratory by electron beam radiation, applying the PIPS process. Comparison of the LS data with theoretical results show two different possibilities. On the one hand, the RGA and the ADA models for isotropic spheres of 0.5 μm radius fit the data quite well, although the ADA seems to be slightly better. On the other hand, the theory developed by Meeten *et al.* within the RGA appears to be a good description for anisotropic spheres of radius 0.3 μm.

It is clear that the data available so far do not permit us to conclude which model better describes the system under consideration. Further measurements using light scattering and other complementary techniques such as

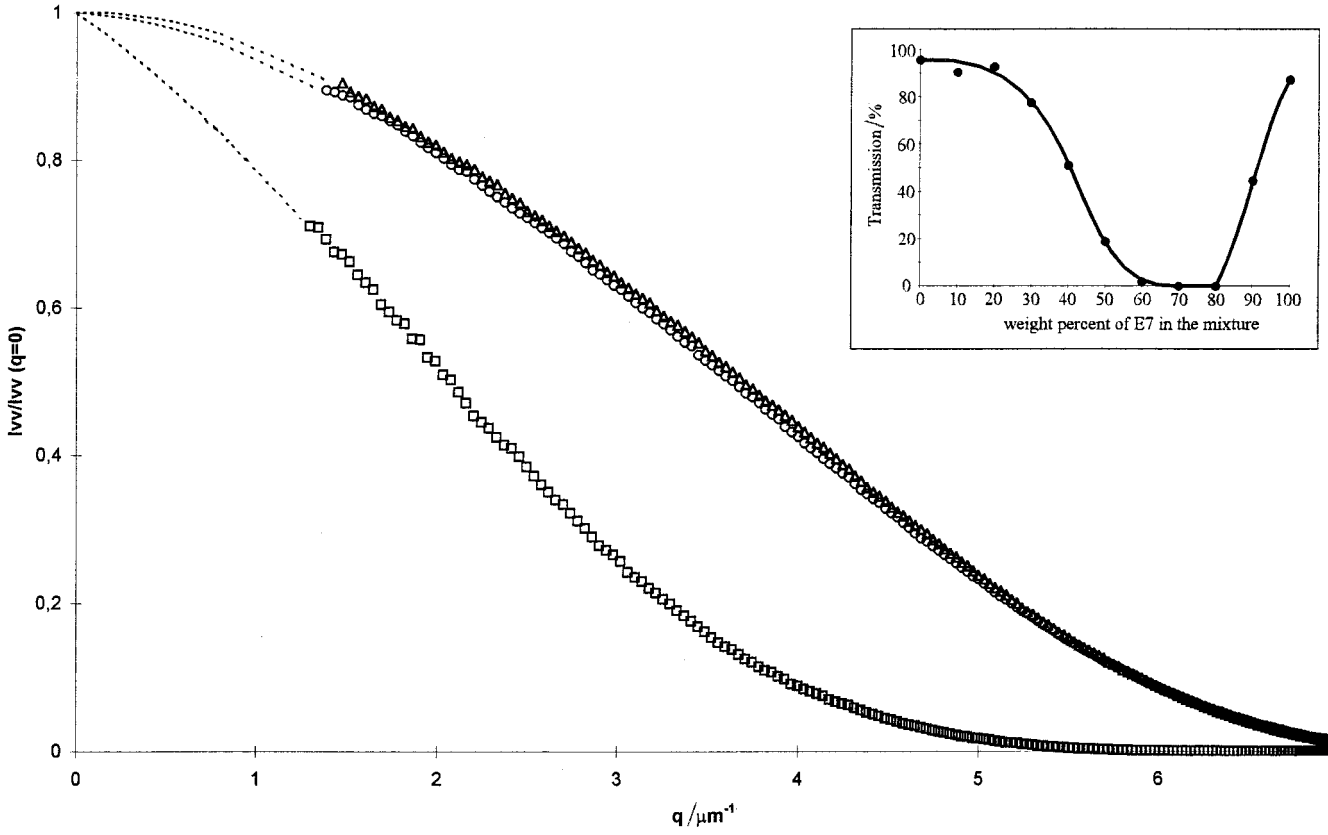

Figure 6. Light scattering data giving $I_{VV}(\mathbf{q})/I_{VV}(\mathbf{q}=0)$ as a function of $\mathbf{q}$ for PDLC systems based on the polyacrylate/E7 system at three different LC concentrations. ○ : 50 wt % LC; △: 60 wt % LC; □ : 70 wt % LC. The figure inset represents transmission data for the same system [8].

scanning electron microscopy and light transmission could enable us to draw more definite conclusions. The relative consistency between light scattering and transmission data for different LC compositions provides a good incentive for undertaking more systematic studies on various PDLC systems under similar conditions. This would help to reach more definite conclusions concerning the possible correlation between the results obtained from all these experiments.

The first author gratefully acknowledges the MPG and the CNRS for financial support during his stay at the MPI-P in Mainz where this work has been accomplished. We also thank Prof. Dr Joe B. Whitehead for correspondence which helped to clarify some issues of this paper.

References

[1] Doane, J. W., 1990, *Liquid Crystals—Applications and Uses*, edited by B. Bahadur (Singapore: World Scientific), Vol. 1, Chap. 14.
[2] Kitzerow, H. S., 1994, *Liq. Cryst.*, **16,** 1.
[3] Drzaic, P. S., 1995, *Liquid Crystal Dispersions* (Singapore: World Scientific).
[4] 1996, *Liquid Crystals in Complex Geometry*, edited by G. P. Crawford and S. Zumer (London: Taylor & Francis).
[5] Bouteiller, L., and Le Barny, P., 1996, *Liq. Cryst.*, **21,** 157.
[6] Maschke, U., Coqueret, C., and Loucheux, 1995, *J. appl. Polym. Sci.*, **56,** 1547.
[7] Maschke, U., Gloaguen, J.-M., Turgis, J.-D., and Coqueret, X., 1996, *Mol. Cryst. liq. Cryst.*, **282,** 407.
[8] Maschke, U., Traisnel, A., Turgis, J.-D., and Coqueret, X., 1997, *Mol. Cryst. liq. Cryst.*, **299,** 371.
[9] Maschke, U., Gogibus, N., Traisnel, A., and Coqueret, X., 1997, *Liq. Cryst.*, **23,** 457.
[10] Lord Rayleigh, 1871, *Philos. Mag.*, **41,** 107; 274; 447.
[11] Gans, R., *Ann. Phys.*, 1925, **76,** 29.
[12] Van De Hulst, H. C., 1957, *Light Scattering by Small Particles* (New York: John Wiley & Sons).
[13] Stein, R. S., and Rhodes, M. B., 1960, *J. appl. Phys.*, **31,** 1873.
[14] Meeten, G. H., 1982, *Opt. Acta.*, **29,** 759.
[15] Meeten, G. H., and Navard, P., 1984, *J. Polym. Sci., Polym. Phys. Ed.*, **22,** 2159.
[16] Champion, J. V., Killey, A., and Meeten, G. H., 1985, *J. Polym. Sci., Polym. Phys. Ed.*, **23,** 1467.
[17] Meeten, G. H., and Navard, P., 1989, *J. Polym. Sci., Polym. Phys. Ed.*, **27,** 2023.
[18] Zumer, S., and Doane, J. W., 1986, *Phys. Rev. A*, **34,** 3373.

[19] ZUMER, S., 1988, *Phys. Rev. A*, **37,** 4006.
[20] ZUMER, S., GOLEMME, A., and DOANE, J. W., 1989, *J. opt. Soc. Am. A*, **6,** 403.
[21] WHITEHEAD, JR., J. B., ZUMER, S., and DOANE, J. W., 1989, *SPIE*, **1080,** 250.
[22] WHITEHEAD, JR., J. B., ZUMER, S., and DOANE, J. W., 1993, *J. appl. Phys.*, **73,** 1057.
[23] DING, J., and YANG, Y., 1994, *Mol. Cryst. liq. Cryst.*, **257,** 63.
[24] DING, J., and YANG, Y., 1994, *Mol. Cryst. liq. Cryst.*, **238,** 47.
[25] MONTGOMERY, G. P., 1988, *J. opt. Soc. Am. B*, **5,** 774.
[26] MONTGOMERY, G. P., and VAZ, N. A., 1989, *Phys. Rev. A*, **40,** 6580.
[27] BIGANSKA, O., BUDTOVA, T., PEUVEL-DISDIER, E., and NAVARD, P., 1995, *Mol. Cryst. liq. Cryst.*, **261,** 167.
[28] TAHATA, S., TSUMURA, A., MIZUNUMA, M., KAYAMA, H., TAMATANI, A., and MASUMI, T., 1996, *Mol. Cryst. liq. Cryst.*, **275,** 99.
[29] HUANG, Z., CHIDICHIMO, G., NICOLETTA, F. P., DE SIMONE, B. C., and CARUSO, C., 1996, *J. appl. Phys.*, **80,** 6155.
[30] KERKER, M., 1969, *The Scattering of Light and Other Electromagnetic Radiation* (New York: Academic).
[31] BOHREN, C. F., and HOFFMAN, D. R., 1983, *Absorption and Scattering of Light by Small Particles* (New York: Wiley).
[32] MASCHKE, U., DEROUARD, C., GOGIBUS, N., COQUERET, X., ISMAILI, M., JOLY, G., and ISAERT, N., (in preparation).
[33] (*a*) MERCK, 1994, *Licrilite* brochure: (*b*) TARRY, H. A., 1967, *The Refractive Indices of Cyanobiphenyl Liquid Crystals* (Merck Ltd, Merck House, Poole, Great Britain).
[34] ABRAMOWITZ, M., and STEGUN, I. A., 1972, *Handbook of Mathematical functions* (New York: Dover Publications Inc.), p. 376.